Magnetic Resonance Imaging 62 (2019) 220–227

Contents lists available at ScienceDirect

Magnetic Resonance Imaging

journal homepage: www.elsevier.com/locate/mri

Original contribution

Deep learning reveals untapped information for local white-matter fiber reconstruction in diffusion-weighted MRI

Vishwesh Nath[a,*], Kurt G. Schilling[b], Prasanna Parvathaneni[c], Colin B. Hansen[a], Allison E. Hainline[d], Yuankai Huo[b], Justin A. Blaber[c], Ilwoo Lyu[a], Vaibhav Janve[e], Yurui Gao[e], Iwona Stepniewska[f], Adam W. Anderson[e], Bennett A. Landman[a,b,c]

[a] Computer Science, Vanderbilt University, Nashville, TN, USA
[b] Biomedical Engineering, Vanderbilt University, Nashville, TN, USA
[c] Electrical Engineering, Vanderbilt University, Nashville, TN, USA
[d] Biostatistics, Vanderbilt University, Nashville, TN, USA
[e] Vanderbilt University Institute of Imaging Science, Vanderbilt University Medical Center, Nashville, TN, USA
[f] Psychology, Vanderbilt University, Nashville, TN, USA

ARTICLE INFO

Keywords:
DW-MRI
HARDI
Deep learning
Spherical harmonics
Histology
Ground truth

ABSTRACT

Purpose: Diffusion-weighted magnetic resonance imaging (DW-MRI) is of critical importance for characterizing in-vivo white matter. Models relating microarchitecture to observed DW-MRI signals as a function of diffusion sensitization are the lens through which DW-MRI data are interpreted. Numerous modern approaches offer opportunities to assess more complex intra-voxel structures. Nevertheless, there remains a substantial gap between intra-voxel estimated structures and ground truth captured by 3-D histology.

Methods: Herein, we propose a novel data-driven approach to model the non-linear mapping between observed DW-MRI signals and ground truth structures using a sequential deep neural network regression using residual block deep neural network (ResDNN). Training was performed on two 3-D histology datasets of squirrel monkey brains and validated on a third. A second validation was performed using scan-rescan datasets of 12 subjects from Human Connectome Project. The ResDNN was compared with multiple micro-structure reconstruction methods and super resolved-constrained spherical deconvolution (sCSD) in particular as baseline for both the validations.

Results: Angular correlation coefficient (ACC) is a correlation/similarity measure and can be interpreted as accuracy when compared with a ground truth. The median ACC of ResDNN is 0.82 and median ACC's of different variants of CSD are 0.75, 0.77, 0.79. The mean, median and std. of ResDNN & sCSD ACC across 12 subjects from HCP are 0.74, 0.88, 0.31 and 0.61, 0.71, 0.31 respectively.

Conclusion: This work highlights the ability of deep learning to capture linkages between ex-vivo ground truth data with feasible MRI sequences. The data-driven approach is applicable to human in-vivo data and results in intriguingly high reproducibility of orientation structure.

1. Introduction

Precise reconstruction of white-matter (WM) structural connectivity is of critical importance for the advancement of neuroscience. Though multiple approaches have been proposed for the reconstruction of WM micro-structure a consensus for precision and reproducibility has not been attained [1]. A critical challenge when reconstructing WM connectivity for human MRI in-vivo acquisitions is due to the lack of a ground truth [2,3]. Multiple approaches have been proposed to reconstruct WM micro-structure and resolve multiple fiber orientations per voxel in the brain [4,5]. Here, we address two key questions: 1) 'Do state-of-the-art methods precisely capture independently observed structure? (Fig. 1)' and 2) 'Are data-driven approaches able to better capture this structure while generalizing for in-vivo data?'

Diffusion tensor imaging (DTI) [6] is a diffusion-weighted magnetic resonance imaging (DW-MRI) technique that has been widely applicable for clinical and research use. DTI can only resolve a single direction of fiber structure [7,8], but it is well known that more complex structures are pervasive, such as crossing and fanning fibers [9,10]. To resolve complex structures multiple classical approaches have been

* Corresponding author at: Vanderbilt University, USA.
E-mail address: vishwesh.nath@vanderbilt.edu (V. Nath).

https://doi.org/10.1016/j.mri.2019.07.012
Received 28 March 2019; Received in revised form 29 June 2019; Accepted 14 July 2019

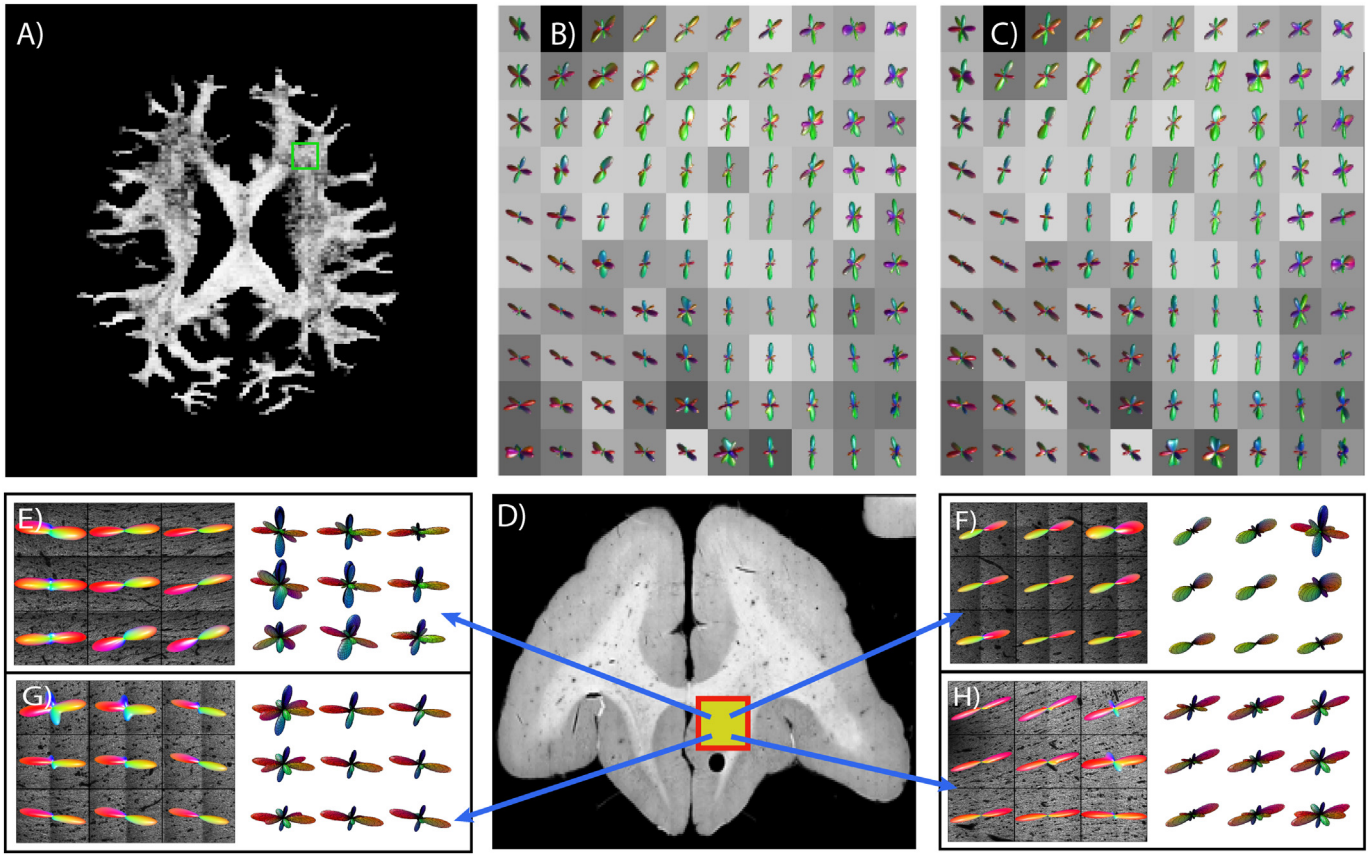

Fig. 1. A) Middle axial slice of a human brain acquired using DW-MRI. B, C) CSD FOD's of the same subject on two different scanners showing inconsistency which cannot be validated without ground truth. D) Coronal slice of a Squirrel Monkey. E, F, G, H) Right: CSD FOD's at b-value of 3000 s/mm^2 Left: Ground truth reconstruction using aggregated histological structural tensors depicting a loss in precision.

proposed such as CSD, Q-ball, PAS-MRI [5,11–15]. The proposed approaches are often collectively termed as high-angular resolution diffusion imaging (HARDI) methods [16], but HARDI methods are plagued by limited reproducibility and are difficult to assess with respect to precision due to the challenge of lack of a ground truth. Validation studies have highlighted biases, inaccuracies, and limitations of HARDI methods in characterizing tissue microstructure [17]. This gap in performance suggests that DW-MRI signal may not be utilized completely/sufficiently.

Data-driven approaches can be useful in validation of the hypothesis of the existence of untapped information because they generalize towards the ground truth. Deep learning has become a critical tool as a subset of machine learning and has recently been introduced in MRI reconstruction as well. Generative adversarial networks have been used for acceleration of reconstruction of MRI [18]. The authors couple the adversarial loss with an innovative content loss. While [19] uses the introduced novelty above, additionally they propose to use a two-stage architecture for better adaption of loss functions and ensure learning on other features as compared to joint training. The results were interpreted on a cardiac MRI dataset. Deep learning has also been applied to diffusion tensor cardiac magnetic resonance for resolving microscopic structural organization of the myocardium [20]. A cascaded convolutional neural network architecture was used for assessment as compared to other classical methods on a simulated dataset. Herein, we apply deep learning to show evidence of untapped information in DW-MRI signal. Deep learning in general has been particularly useful in generalizing non-linear mappings [21]. Herein, we show the evidence of untapped information using a residual deep learning neural network (ResDNN) based on prior work [24]. Our network was trained on a 3-D confocal histology dataset consisting of white matter (WM) voxels from two squirrel monkey brains and validated on a third, independent brain [17]. Further we also show an improvement in terms of reproducibility when the newly created method is applied on scan-rescan data from in-vivo human brain DW-MRI acquisitions from the Human Connectome Project (HCP). The DNN applicable for reconstruction of local white matter reconstruction was first proposed in [24].

This study presents the first data-driven diffusion-weighted magnetic resonance imaging (DW-MRI) analysis method that links in-vivo feasible imaging protocols with 3-D histological ground truth. A novelty here is an introduction of combined usage of histology and deep-learning. Under full-specimen validation, the proposed model yields higher predictive accuracy than the leading model-based approach. Hence, this study demonstrates that a significant level of information in the DW-MRI is untapped with current analysis methods. Moreover, we demonstrate that the proposed method is more reproducible in a sample of scan-rescan pairs from the Human Connectome Project. The proposed method generalizes from an ex-vivo pre-clinical context to an in-vivo human context without re-training.

2. Methods

2.1. Squirrel monkey data acquisition

All animal procedures were approved by the Vanderbilt University Animal Care and Use Committee. This data comes from a prior study [17]. Three ex-vivo squirrel monkey brains were imaged on a Varian 9.4 T scanner. A total of 100 gradient volumes were acquired using a diffusion-weighted echo planar imaging (EPI) sequence at a diffusivity value of 9000 s/mm^2 with the isotropic resolution being 0.3 mm. Once acquired the tissue was sectioned and stained with fluorescent dil and

imaged on a LSM710 Confocal microscope followed [17]. The histological fiber orientation distribution was extracted using 3D structure tensor analysis [17]. A multi-step registration procedure was used to determine the corresponding diffusion MRI signal. A total of 567 histological voxels were processed. Respective number of voxels by Monkey A, B and C were 270, 162 and 135. 54 of the total number of voxels were labelled as outliers qualitatively and rejected for analysis. The outlier voxels were detected using ACC when fitted with sCSD. A hundred random rotations were applied to the remaining voxels after the removing the outliers. This brought the total number of voxels to 51,813 voxels. All voxels from Monkey C were kept completely hidden for evaluation purpose of the machine learning model. Total number of voxels for Monkey C after outlier removal were 9090. The voxels from monkey A and B were used for the training and they accumulated to a total of 42,723.

Each random rotation is defined by 3D rotation from axis and angle followed using [22]. The same random rotation was applied to both the input signal and the output FOD to ensure integrity of the data. The multi-step registration procedure has been adapted from existing prior work [23]. Deep learning requires the usage of a large dataset. The most common classification datasets of in machine learning are MNIST and CIFAR consist of 60,000 images. Data augmentation with such datasets have been known to improve performance of deep learning algorithms. Traditional augmentation techniques such as additive noise, image shearing, flipping and rotation et cetera have been known to work well. For the specific case of this work of the afore mentioned techniques 3D rotation augmentation would be the most applicable as a single set of SH coefficients represent a geometric structure. Hence, corresponding random rotations to diffusion coefficients and histology structure coefficients would be the most applicable. The immediate advantage that one would obtain is having an increased number of data points which is beneficial for deep learning algorithms. Disadvantages for data augmentation only occur in a rare scenario where it might lead to overfitting of data.

2.2. Human connectome project data

Human connectome project (HCP) data of 12 subjects with the retest acquisition was used (ID's: 103818, 105923, 111312, 114823, 115320, 122317, 125525, 130518, 139839, 143325, 144226 and 146129). The acquisitions at b-value of 3000 s/mm^2 with 90 gradient directions were extracted for the study. A T1 volume of the same subject was used for WM segmentation using FAST [24]. Pre-processed HCP diffusion data was used where topup and eddy have been applied for distortion corrections [25,26].

2.3. Residual deep neural network regression

The data driven models learn a set of parameters when provided with a set of corresponding inputs and outputs. The set of parameters here depict a non-linear mapping. The input was defined by spherical harmonic (SH) coefficients that were fitted to the ex-vivo DW-MRI acquisition of squirrel monkeys per voxel. This was done using regularized linear least squares fit on the DW-MRI signal. The SH coefficients have been known to characterize the diffusion signal sufficiently [27]. Ortho-normal representation allows for flexibility of different acquisitions. SH have also been used for other deep learning based approaches [28–31]. The DW-MRI signal was fitted to 8th order SH [11,27]. Acquisitions with > 45 gradient volumes are known to be characterized well by 8th order SH coefficients. The output for the training network were SH coefficients of 8th order per voxel depicting the fiber orientation distribution (FOD) structure from histology. These were derived from histology [17].

The neural network architecture briefly is five layers deep with the number of neurons per layer being: 45 (Input), 400, 45, 200, 45, 200 and 45 (Output) respectively (Fig. 2). The alternating number of neuron architecture was inspired from prior work on signal augmentation using deep learning coupled with spherical harmonics [28]. The premise of this work was to predict multi-shell signal from single-shell. The current work is focused on recovering the microstructure which is also represented as spherical harmonics (SH). The ResDNN network has a residual block for the middle three layers to ensure robustness to prevent overfitting. Rectified linear units were used for activation only to introduce non-linearity. The output layer was not activated to introduce negativity in the ResDNN as SH coefficients can be negative. Default hyper-parameters of 'RMSProp' optimizer were used while training the network for convergence with the exception of learning rate being set to 10^{-4} [32]. Cross-validation set size was set to 0.2. Number of iterations for optimal convergence were determined to be at 400.

A NVIDIA Titan Xp with 11GB of memory with an Ubuntu 16.04 LTS workstation was used for running the experiments. The training time taken for this network is < 10 min and the prediction time on a whole volume of the brain after fitting spherical harmonic coefficients is approximately 2 min. Source code and trained model weights are available on: https://github.com/finalelement/dl_untapped_info_dwmri_histo.

2.4. HARDI methods and angular correlation coefficient

Multiple HARDI methods were implemented for comparison to the proposed ResDNN approach. A list of methods that were compared for the acquisition of the test monkey 'C' are Q-ball imaging (QBI), with constant solid angle (QBICS), super resolved constrained spherical deconvolution (sCSD) at 6th and 8th order, Lucy-Richardson constrained spherical deconvolution (CSDLR), diffusion orientation transform (DOT), diffusion orientation transform revisited (DOTr1). All the mentioned HARDI methods were compared using angular correlation coefficient (ACC) [15]. ACC is defined as below:

$$ACC = \frac{\sum_{j=1}^{\infty}\sum_{m=-j}^{j} u_{jm} v_{jm}^{*}}{\left[\sum_{j=1}^{\infty}\sum_{m=-j}^{j} |u_{jm}|^2\right]^{0.5} \cdot \left[\sum_{j=1}^{\infty}\sum_{m=-j}^{j} |v_{jm}|^2\right]^{0.5}} \quad (2)$$

ACC is calculated using 'u' and 'v' where they are two sets of SH coefficients of the same order. ACC is measure of similarity on a scale of −1 to 1. A measurement of 1 denotes a perfect similarity.

3. Results

Results are presented in three sections: 1) we compare the ground truth histology with HARDI methods and ResDNN with accuracy assessed by ACC [15]. All comparisons were made on a third squirrel monkey which was not used for the training of the network. 2) Quantitative assessment of scan-rescan pairs from HCP dataset using 12 subjects using ACC with sCSD at 6th and 8th order. 3) Qualitative assessment of the fiber orientation distribution (FOD) glyphs and spatial maps of slices from in-vivo HCP brain slices.

A trained ResDNN using ground truth based on histology with corresponding diffusion signal reconstructs more precise fiber structure as compared to sCSD. The median ACC of the ResDNN is 0.82 as compared to any other HARDI method approach where all median is < 0.79 (Fig. 3). Non-parametric signed rank tests for the ACC distributions shows that ResDNN is higher than other HARDI methods ($p \ll 0.01$).

For quantitative assessment on in-vivo DW-MRI acquisitions the ResDNN was tested on paired human in-vivo acquisitions. Twelve test-retest acquisition subjects were acquired from the human connectome project (HCP). The distribution of ACC between the pair of scans for sCSD at 6th order SH, 8th order and SH ResDNN are shown in (Fig. 4). ResDNN shows the most skewed distribution towards higher correlation (Fig. 4A). Observing distribution plots per subject the ResDNN shows a more skewed distribution towards higher correlation for all subjects as

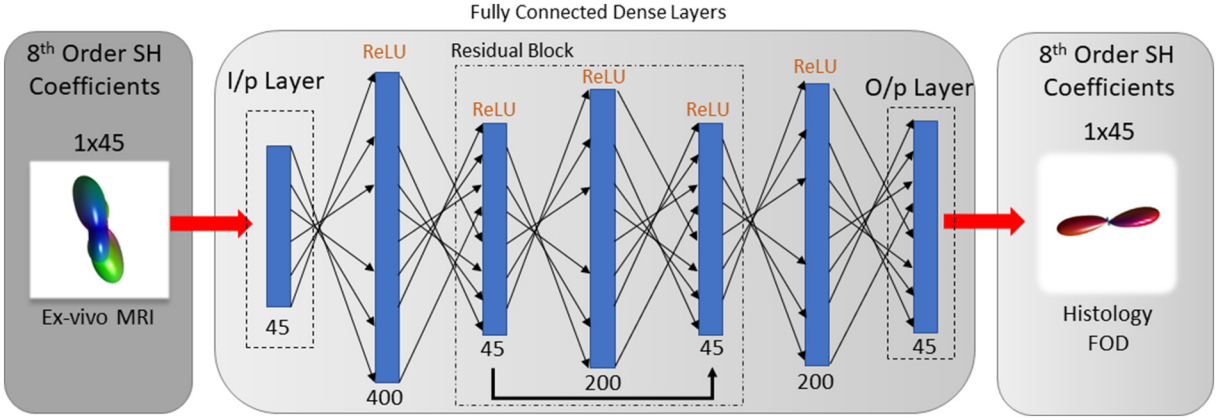

Fig. 2. Left to Right: Input of SH coefficients of DW-MRI signal at 8th order to the DNN. The middle box depicts the architecture of the ResDNN with number of neurons and activation functions respectively. Output is denoted by SH coefficients of the FOD of a structural tensor at 8th order.

compared to sCSD at 6th and 8th order. The mean, median and standard deviation of the ACC across the 12 subjects for CSD at 6th order: [0.61, 0.71, 0.31], 8th order: [0.54, 0.60 and 0.31]. The same for the ResDNN are [0.74, 0.88, 0.31]. The reproducibility gain calculated by the difference of the ACC median of sCSD at 6th order and ResDNN is 24% and the same for 8th order is 46%. Non-parametric signed ranked test for all pairs of ACC distributions show that the ACC of ResDNN is significantly higher than sCSD ($p \ll 0.01$).

We chose a region of interest (ROI) in the right frontal lobe of the white matter (WM) of the brain (Fig. 5). Comparing sCSD (Fig. 5A & B) we can observe that the FOD glyphs are similar qualitatively for single fiber populations; however, notable differences can be seen for multiple fiber populations. Comparing ResDNN (Fig. 5D & E) the FOD glyphs visually agree more as compared to sCSD specifically glyphs with multiple fiber populations as well. Observing the ACC across the middle axial slice of the brain for sCSD (Fig. 5C) and ResDNN (Fig. 5F), it can be noticed that the ACC is higher across the brain for DNN.

Spatial maps of ACC (Fig. 6) show that the ACC for ResDNN predicted SH coefficients are higher for all pairs of subjects when compared with ACC of sCSD at 6th order. Subject 4, 5, 6 and 12 show lower ACC relatively for both ResDNN and sCSD as compared to other subjects.

FOD glyphs (Fig. 7) of sCSD and CSDLR show a spurious detection of fiber population which is not present in the ground truth for single fiber configurations. ResDNN and sCSD both depict similar structure which resembles the ground truth for the principal orientation.

4. Discussion

Accurate characterization of the structural properties of the brain

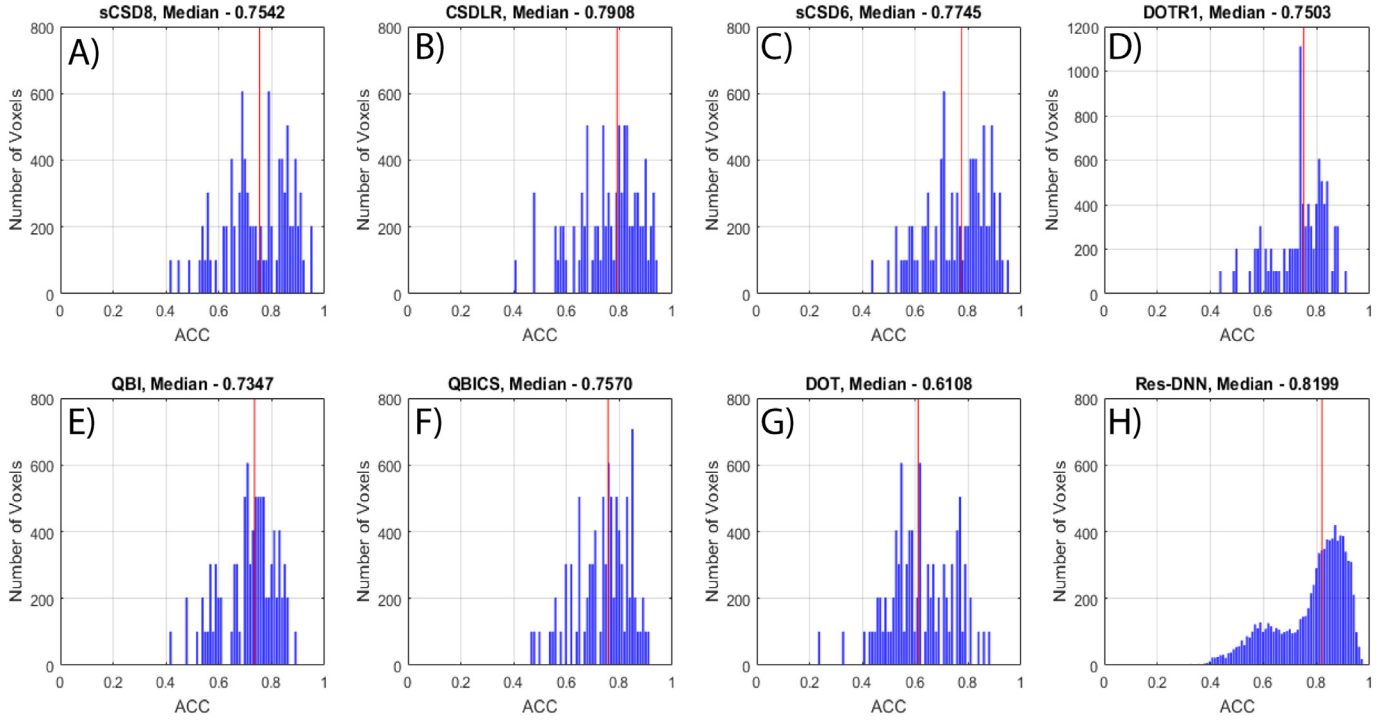

Fig. 3. Distribution of ACC between the ground truth and the CSD FOD's of monkey C. The red line indicates the median at for the distribution. A, C) super resolved constrained spherical deconvolution at 6th and 8th order respectively with median at 0.75 and 0.77. B) Lucy-richardson constrained spherical deconvolution with median at 0.79. D, G) Diffusion orientation transform and its revisited approach with median at 0.61 and 0.75 respectively. E, F) Q-ball imaging and with constant solid angle with median at 0.73 and 0.75. H) Proposed ResDNN approach with median at 0.82. (For interpretation of the references to colour in this figure legend, the reader is referred to the web version of this article.)

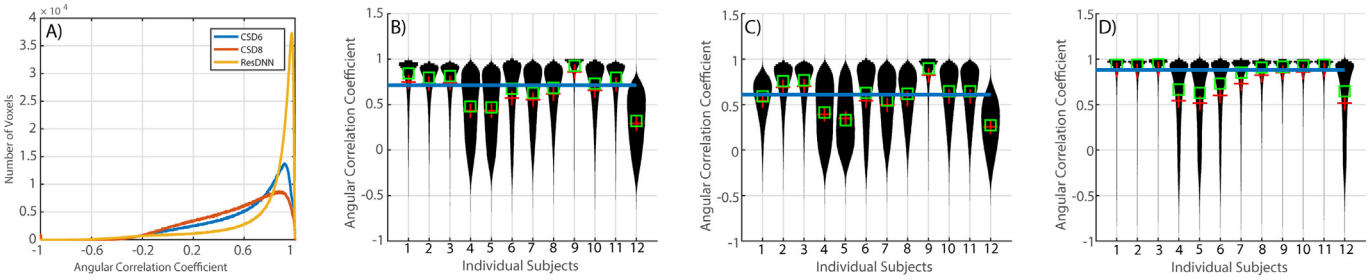

Fig. 4. A) ACC of all paired WM voxels across the 12 subjects laid out in distribution for the ResDNN, sCSD at 6th and 8th order. ResDNN distribution is skewed towards higher correlation. B, C, D) Violin plots per subject of ACC for paired WM voxels for sCSD at 6th order, 8th order and ResDNN. Blue line denotes the median. (For interpretation of the references to colour in this figure legend, the reader is referred to the web version of this article.)

can lead to fundamental insights into cognition, development, and diseases. Currently, the only noninvasive method to map the structural connectivity is diffusion MRI. In this study, we use data-driven machine learning approaches to learn a relationship between the diffusion MRI signal and the underlying tissue microstructure. Together, we find that there is information in the diffusion signal that is currently unutilized or underutilized by current methods, and that this information is stable. Specifically, our study has three major takeaways: 1) ResDNN can reconstruct the FOD more precisely/accurately than current diffusion reconstruction methods. 2) The information gain is significant which is indicative of a more precise reconstruction of the micro-structure architecture of the brain, while also providing evidence that a better non-linear mapping exists between the signal and the FOD. 3) In-vivo validation on scan and rescan data used from the HCP confirms reproducibility and stability of the model, demonstrating clinical applicability. Qualitative analysis re-enforces the improved scan-rescan consistency.

While advocating the use of a data-driven approach is nascent in the domain of DW-MRI. A novelty here is the introduction of the combined usage of histology and deep-learning. The numerous classical approaches to reconstruct the FOD have been reproducible and successful however the evidence suggests that a more precise one could be discovered. The result of the information gain shows us that there is untapped information present in the DW-MRI signal that is not being accounted for. This study in no way suggests as to what could be another non-linear mapping. The advancements in machine-learning specifically deep learning have made this discovery possible.

Deep learning has been widely applicable in image processing and has become a powerful tool. While it is still treated as a black box because of the large number of parameters that a ResDNN learns, deep learning is becoming clinically accepted. Although a simple sequential ResDNN has been used for the study, more complex networks can be designed for more specific DW-MRI problems. Spatial information as features can be used for improving the performance of the ResDNN. A precise reconstruction of FOD's directly leads to improved performance for tractography algorithms.

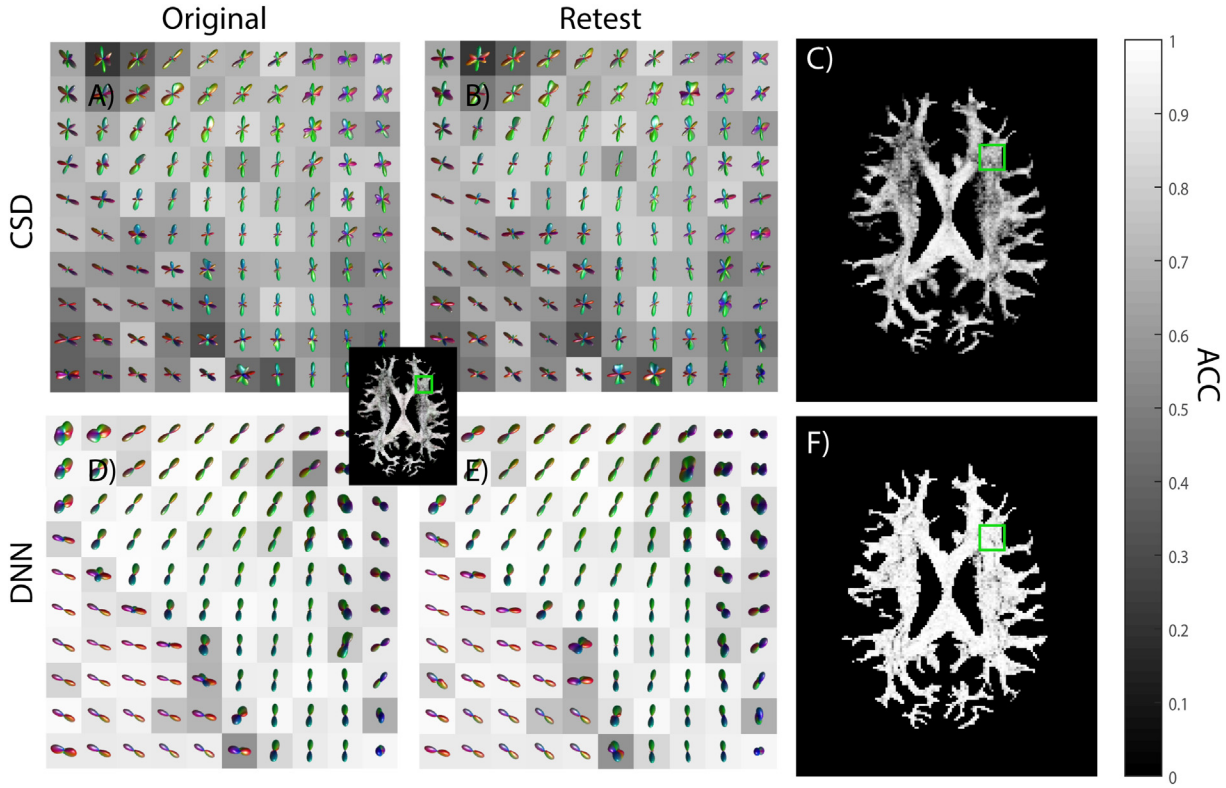

Fig. 5. The selected ROI shows frontal lobe of WM on right side. The image underlay in A, B, D & E is ACC which shows agreement between pairs of A & B and D & E. C & F show the ACC of the middle axial slice of the brain. FOD of sCSD are shown in A & B where they show lesser agreement as compared to FOD of ResDNN in D & E.

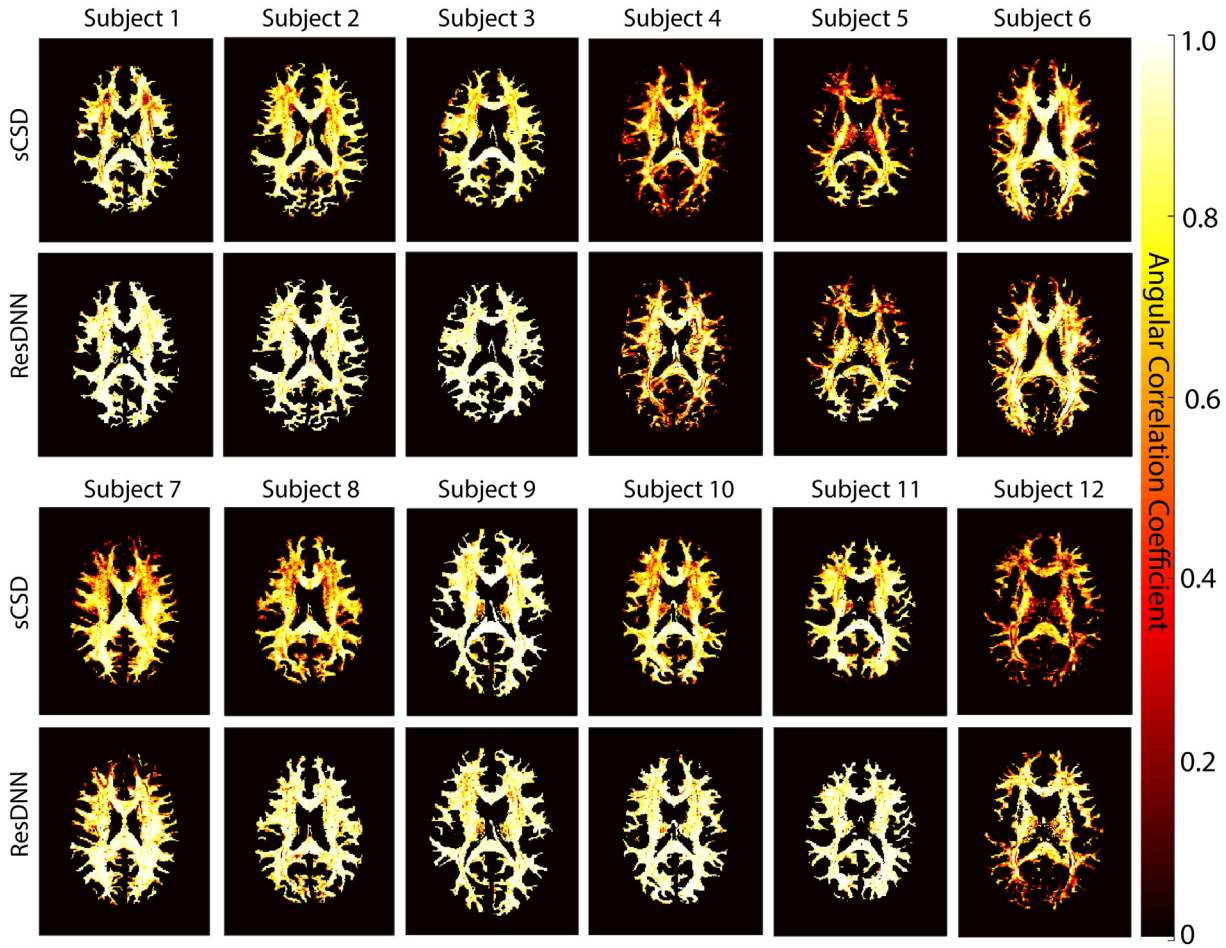

Fig. 6. Spatial maps of ACC of middle axial slice for scan-rescan pairs are shown for both ResDNN and sCSD at 6th order. First row shows sCSD ACC spatial maps for subjects 1–6. Second row shows ResDNN ACC spatial maps for subjects 1–6. Third row shows sCSD ACC spatial maps for subjects 7–12. Fourth row shows ResDNN ACC spatial maps for subjects 7–12. It can be observed that the ResDNN shows higher ACC for all observed pairs.

On a side note there are multiple HARDI methods that enforce non-negativity in different ways [14,33]. However, they cannot be directly enforced upon deep learning, hence to enforce non-negativity we follow a proposed procedure (Fig. 8A). Starting out with normalized DW-MRI signal it is truncated by a regularizing hyper-parameter (theta = 0.005). This is needed to eliminate negative and extremely low values (< 0.005) as they would translate to noisy values in log transform. The log transform of DW-MRI signal was fitted to SH leading to them being in log space. This procedure was performed on the FOD SH coefficients as well. A consistent set of 100 gradient directions was used which uniformly sampled over a sphere. While testing the withheld set of voxels were not transformed in any way to ensure integrity of blind testing. In comparison the non-negative results show a median ACC of 0.81 as compared to ResDNN ACC of 0.82. While there is a little compensation in correlation, we are able to enforce non-negativity in the network. The non-negativity requires a deeper validation to show further applicability. While there are still limitations to this work.

This focus of this work has been on using histology to learn the relationship between the observed MRI signal and an external source of microstructure truth. The validation has been in terms of accuracy relative to withheld voxels and reproducibility with scan-rescan imaging. As yet, we have not sought validation in terms of external imaging modality. Since we use confocal imaging along with MRI, the joint relationship that we learn is external to neither [34]. An independent characterization would imbue greater confidence, but could also be used along with learning process to improve accuracy. The dilemma of using data for validation versus learning is ever present as we balance bias/variance tradeoffs is modern machine learning. On another front, validation of clinical utility is open problem. We have shown that the metrics that can be learned are more consistent with histology than traditional diffusion/FOD modeling; however, we have not shown that these more accurate models are indeed more sensitive/specific to a disease pathology. We have made both the models and the source code available to enable these studies as we ourselves also continue to explore application of these models.

An important point of discussion is the contrast in DW-MRI images when comparing ex-vivo and in-vivo imaging data. A known effective pipeline when making comparisons for ex-vivo and in-vivo imaging data has been shown in [35]. It is known that tissue properties vary after death however the diffusivity measure have been retained for periods of up to 3 years as shown in [35]. The work also discusses the important aspect of b-values for ex-vivo acquisitions that would allow optimal tissue reconstruction. It has been suggested that b-values approximately in the range 2000–8000 s/mm^2 work out well with the optimal b-value being suggested at 4000 s/mm^2. However, it should also be accounted that PAS-MRI was used for tissue reconstruction and the specific method is known to function well at lower b-values as well.

This work could be improved with further applicability shown to post-mortem human ex-vivo data. However, such datasets are rare and the analysis has not been presented due to lack of such datasets. Assuming presence of such datasets it would lead us to more precise and informative reconstructions of the white matter tissue structure. The reconstruction would also lead to well-validated and precise tractography based reconstructions for human white matter tissue

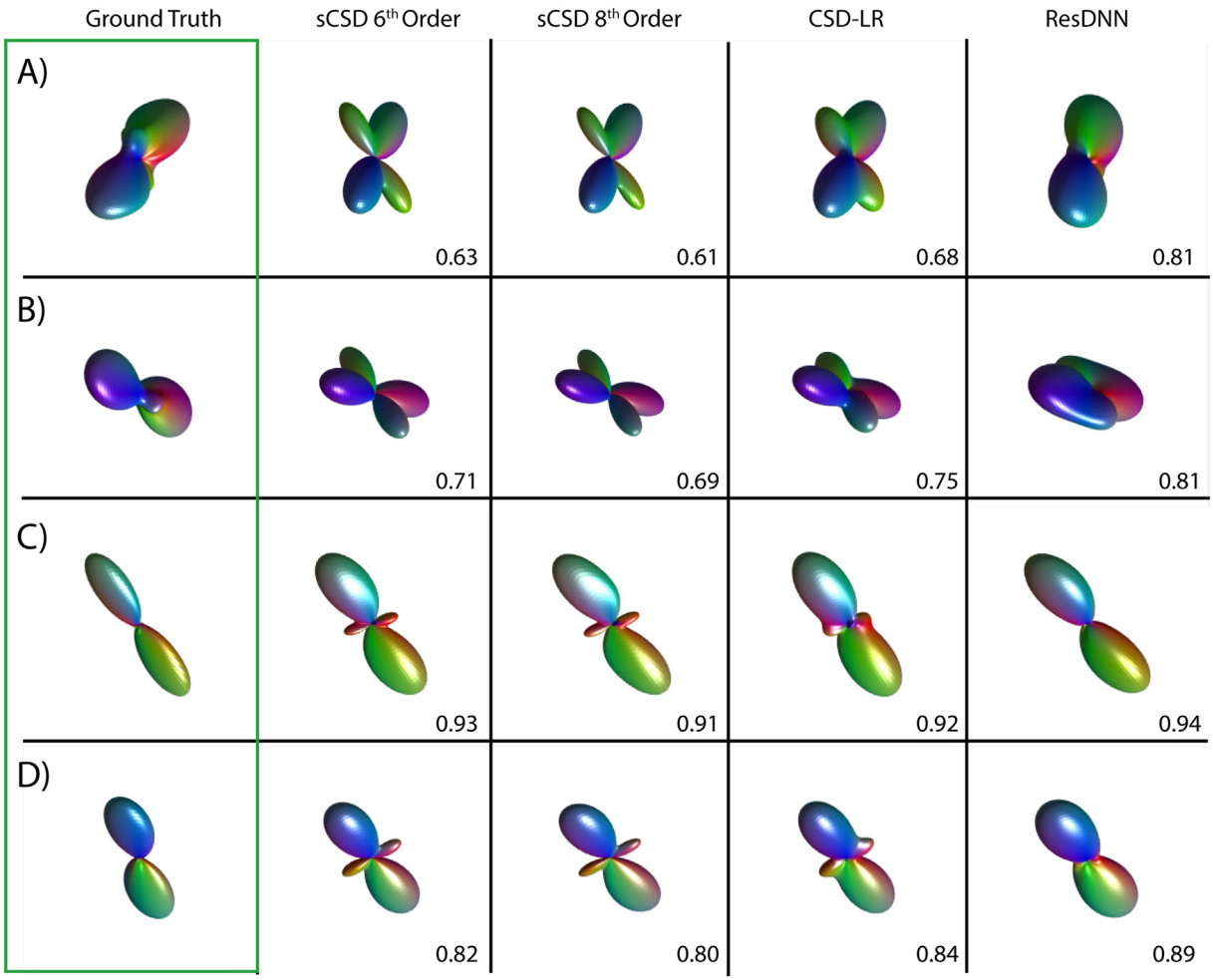

Fig. 7. A, B, C, D) 1st Column: depicts ground truth FOD with representation as 8th order SH Coefficients. 2nd & 3rd Column: depicts sCSD predicted FOD with representation of 6th and 8th order SH. 4th Column: depicts CSDLR predicted FOD with representation as 8th order SH. 5th Column: depicts ResDNN predicted FOD as 8th order SH Coefficients. ACC is depicted at bottom right corner when compared with ground truth.

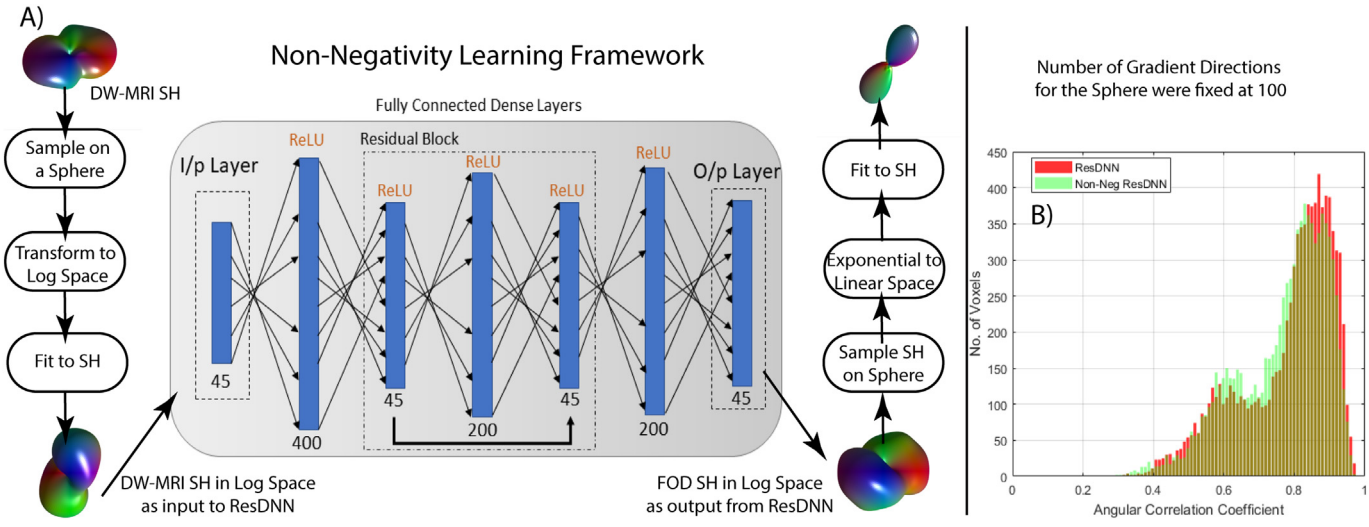

Fig. 8. A) Describes the step procedure followed to incorporate non-negativity which consists of a log transformation to eliminate negative values and using log space SH coefficients for input and output for ResDNN network. B) Shows the comparison between the ground truth and predictions from ResDNN in linear space and log space.

microarchitecture.

Apart from precision the criteria of reproducibility have been validated as well using scan-rescan pairs from the HCP. Reproducibility while not correlated with precision has its own independent importance due to the fact of clinical applicability. Precision without reproducibility is an example of high variance in the information being

reconstructed. For example, if the reproducibility is not high for a healthy control subject then the interpretation of the reconstruction on a diseased subject would be an unreliable one. Here we have shown that the ResDNN achieves high reproducibility across two different datasets: HCP and in-house acquired data. This work marks an initial advent of artificial intelligence (AI) in DW-MRI.

AI has gained quite the popularity and applicability in multiple domains. The ResDNN presented here can be foreseen as a small part of an overall data-driven approach that could eventually be constructed for DW-MRI data. There are multiple clinical issues regarding DW-MRI that can be tackled such handling of multiple acquisition hyper-parameters and acquisition details.

The ResDNN presented can only learn as well as the presented ground truth to it which could be improved upon (improved registration, SNR, artifact suppression, etc.). Also, another limitation is that the DW-MRI acquisition was ex-vivo for the training of the ResDNN. However, it was validated upon human in-vivo data. Lastly, the dataset that was created was sparse. Standard data augmentation techniques could possibly be useful in making the dataset usable for training this model for the study. We hope that the work presented in this study will be helpful in guiding researchers and neuroscientists better for forward looking research in AI with DW-MRI.

5. Conclusion

We have shown three key findings with the presented study. 1.) A machine learning framework can be used to directly learn the non-linear mapping between DW-MRI and 3D confocal histological derived ground truth. 2.) The trained ResDNN is able to show that it is able to utilize untapped information which is present in the DW-MRI signal. 3.) The trained ResDNN model is able to perform more consistently when relatively compared to state of the art sCSD.

Acknowledgements

This work was supported by R01EB017230 (Landman), RO1NS058639 (Anderson), S10RR17799 (Gore) and T32EB001628. This work was conducted in part using the resources of the Advanced Computing Center for Research and Education at Vanderbilt University, Nashville, TN. This project was supported in part by the National Center for Research Resources, Grant UL1 RR024975-01, and is now at the National Center for Advancing Translational Sciences, Grant 2 UL1 TR000445-06. The content is solely the responsibility of the authors and does not necessarily represent the official views of the NIH.

References

[1] Le Bihan D. Looking into the functional architecture of the brain with diffusion MRI. Nat Rev Neurosci 2003;4(6):469.
[2] Le Bihan D, et al. Artifacts and pitfalls in diffusion MRI. J Magn Reson Imaging 2006;24(3):478–88.
[3] Jones DK, Cercignani M. Twenty-five pitfalls in the analysis of diffusion MRI data. NMR Biomed 2010;23(7):803–20.
[4] Lenglet C, et al. Mathematical methods for diffusion MRI processing. Neuroimage 2009;45(1):S111–22.
[5] Daducci A, et al. Quantitative comparison of reconstruction methods for intra-voxel fiber recovery from diffusion MRI. IEEE Trans Med Imaging 2014;33(2):384–99.
[6] Basser PJ, Mattiello J, LeBihan D. MR diffusion tensor spectroscopy and imaging. Biophys J 1994;66(1):259–67.
[7] Landman BA, et al. Effects of diffusion weighting schemes on the reproducibility of DTI-derived fractional anisotropy, mean diffusivity, and principal eigenvector measurements at 1.5 T. Neuroimage 2007;36(4):1123–38.
[8] Farrell JA, et al. Effects of signal-to-noise ratio on the accuracy and reproducibility of diffusion tensor imaging–derived fractional anisotropy, mean diffusivity, and principal eigenvector measurements at 1.5 T. J Magn Reson Imaging 2007;26(3):756–67.
[9] Nath V. Empirical estimation of intra-voxel structure with persistent angular structure and Q-ball models of diffusion weighted MRI. 2017.
[10] Nath V, et al. Comparison of multi-fiber reproducibility of PAS-MRI and Q-ball with empirical multiple b-value HARDI. Medical imaging 2017: Image processing. International Society for Optics and Photonics; 2017.
[11] Descoteaux M, et al. Regularized, fast, and robust analytical Q-ball imaging. Magn Reson Med 2007;58(3):497–510.
[12] Tuch DS. Q-ball imaging. Magn Reson Med 2004;52(6):1358–72.
[13] Jansons KM, Alexander DC. Persistent angular structure: new insights from diffusion magnetic resonance imaging data. Inverse Prob 2003;19(5):1031.
[14] Tournier J-D, Calamante F, Connelly A. Robust determination of the fibre orientation distribution in diffusion MRI: non-negativity constrained super-resolved spherical deconvolution. Neuroimage 2007;35(4):1459–72.
[15] Anderson AW. Measurement of fiber orientation distributions using high angular resolution diffusion imaging. Magn Reson Med 2005;54(5):1194–206.
[16] Descoteaux, M., High angular resolution diffusion imaging (HARDI). Wiley encyclopedia of electrical and electronics engineering, 2015.
[17] Schilling K, et al. Comparison of 3D orientation distribution functions measured with confocal microscopy and diffusion MRI. Neuroimage 2016;129:185–97.
[18] Yang G, et al. DAGAN: deep de-aliasing generative adversarial networks for fast compressed sensing MRI reconstruction. IEEE Trans Med Imaging 2017;37(6):1310–21.
[19] Seitzer M, et al. Adversarial and perceptual refinement for compressed sensing MRI reconstruction. International conference on medical image computing and computer-assisted intervention. Springer; 2018.
[20] Schlemper J, et al. Stochastic deep compressive sensing for the reconstruction of diffusion tensor cardiac MRI. International conference on medical image computing and computer-assisted intervention. Springer; 2018.
[21] LeCun Y, Bengio Y, Hinton G. Deep learning. nature 2015;521(7553):436.
[22] Arvo J. Graphics gems II. Elsevier; 2013.
[23] Choe AS, et al. Accuracy of image registration between MRI and light microscopy in the ex vivo brain. Magn Reson Imaging 2011;29(5):683–92.
[24] Zhang Y, Brady M, Smith S. Segmentation of brain MR images through a hidden Markov random field model and the expectation-maximization algorithm. IEEE Trans Med Imaging 2001;20(1):45–57.
[25] Andersson JL, Skare S, Ashburner J. How to correct susceptibility distortions in spin-echo echo-planar images: application to diffusion tensor imaging. Neuroimage 2003;20(2):870–88.
[26] Andersson JL, Sotiropoulos SN. An integrated approach to correction for off-resonance effects and subject movement in diffusion MR imaging. Neuroimage 2016;125:1063–78.
[27] Descoteaux M, et al. Apparent diffusion coefficients from high angular resolution diffusion imaging: estimation and applications. Magn Reson Med 2006;56(2):395–410.
[28] Koppers S, Haarburger C, Merhof D. Diffusion mri signal augmentation: from single shell to multi shell with deep learning. International conference on medical image computing and computer-assisted intervention. Springer; 2016.
[29] Nath V, et al. Inter-scanner harmonization of high angular resolution DW-MRI using null space deep learning. 2018.
[30] Nath, V., et al. SHARD: Spherical harmonic-based robust outlier detection for HARDI methods. in Medical imaging 2018: Image processing. 2018. International Society for Optics and Photonics.
[31] Nath V, et al. Harmonizing 1.5 T/3T diffusion weighted MRI through development of deep learning stabilized microarchitecture estimators. Medical imaging 2019: Image processing. International Society for Optics and Photonics; 2019.
[32] Hinton G, Srivastava N, Swersky K. Neural networks for machine learning-lecture 6a-overview of mini-batch gradient descent. Coursera Lect Slides 2012.
[33] Özarslan E, et al. Mean apparent propagator (MAP) MRI: a novel diffusion imaging method for mapping tissue microstructure. 2013;78:16–32.
[34] Howard AF, et al. Joint modelling of diffusion MRI and microscopy. bioRxiv. 2019. p. 563809.
[35] Dyrby TB, et al. An ex vivo imaging pipeline for producing high-quality and high-resolution diffusion-weighted imaging datasets. 2011;32(4):544–63.